JOURNAL OF ELECTROMAGNETIC ENGINEERING AND SCIENCE, VOL. 22, NO. 3, 344~351, MAY. 2022

https://doi.org/10.26866/jees.2022.3.r.96
ISSN 2671-7263 (Online) · ISSN 2671-7255 (Print)

One-Port Planar Near-Field Antenna Measurement and Corresponding Scatterer Compensation Method

Seunggyu Yang[1] · Kangwook Kim[2,*]

Abstract

A one-port near-field antenna measurement technique with a small wire scatterer is proposed. In the proposed technique, a wire scatterer is scanned with an interval of less than a quarter wavelength, and the measurement is performed at the port of the antenna under test (AUT). A two-dimensional phase unwrapping method is used to remove 180° phase uncertainty. The data obtained in the near-field are transformed to the far-field pattern, and the scattering pattern is compensated for better measurements. The proposed measurement technique was validated by measuring the near-field of an AUT over a planar scanning surface. The far-field radiation pattern obtained using the proposed technique was compared with that obtained from a conventional commercial anechoic chamber. It was observed that they agreed well, especially in the region near the center.

Key Words: Antenna Measurements, Near-Field to Far-Field Transformation, Reciprocity Principle.

I. Introduction

To measure the radiation pattern of an antenna, a two-port measurement system is usually considered. In the two-port measurement system, the antenna under test (AUT) is driven by a known source, and the probe antenna, which is located in the far zone of the AUT, measures the radiation intensity. The radiation pattern of the AUT is obtained directly by tabulating the measured radiation intensity and the angular location of the probe [1]. In millimeter-wave bands, the antenna systems are packaged such that it is difficult to disassemble. If it is necessary to disconnect the radiator antenna from the driving circuitry to measure the radiation pattern, it is difficult to drive the antenna and the radiation characteristics of the antenna would change. In such cases, an indirect antenna measurement technique needs to be considered.

Many antenna systems are electrically large if the mounting platform is included [2, 3]. In such cases, a long distance is required to meet the far zone criteria. In some cases, it may be practically impossible to secure the required distance. Therefore, in this paper, a novel antenna measurement technique is proposed. In the proposed technique, the radiation characteristics are measured using a scatterer that scans in the near-field of the AUT, as shown in Fig. 1. The scattered field is measured by the AUT itself, and the measured quantity is transformed to the far-field pattern using a near-field to far-field transformation (NTFT) method that is proposed in this paper for the one-port measurement method. The proposed measurement technique is advantageous over two-port systems in many aspects. The system hardware configuration is simple. The scatterer can be made

Manuscript received July 16, 2021 ; Revised August 25, 2021 ; Accepted October 25, 2021. (ID No. 20210716-081J)
[1]School of Mechanical Engineering, Gwangju Institute of Science and Technology, Gwangju, Korea.
[2]School of Electrical Engineering and Computer Science, Gwangju Institute of Science and Technology, Gwangju, Korea.
[*]Corresponding Author: Kangwook Kim (e-mail: mkkim@gist.ac.kr)

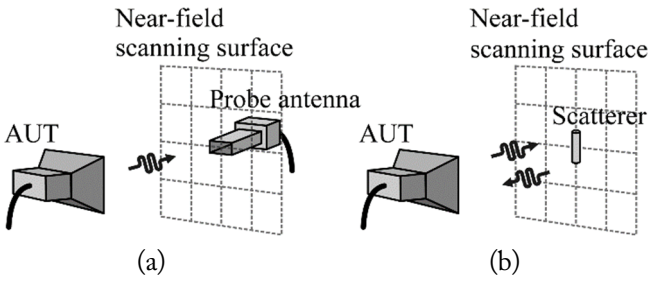

Fig. 1. Near-field antenna measurement concept for (a) two-port system and (b) proposed one-port system.

light weight and, thus, the scanning is easy. There are no moving cables, and the distortion due to the cable can be minimized. Scatterer-based systems have previously been studied [4–6]. However, [4] is only focused on electric field data acquisition, [5] is valid for obtaining a single-plane radiation pattern for linear-polarization and simple aperture antennas, and [6] requires other modulation systems.

In general, the measurement accuracy can be improved by the probe compensation method in a two-port measurement system [7]. Similarly, by compensating the characteristics of the scatterer, the accuracy of the one-port measurement system could be improved. In this paper, a scatterer compensation method for one-port planar NTFT is derived based on the reciprocity theorem. The proposed compensation method is validated through experiment.

II. One-Port Near-Field Antenna Measurement Setup

When two antennas are in the far zone of each other, the relationship between the power received by one antenna and the power transmitted by the other antenna can be simply described by the Friis transmission equation [1]. For the case that each antenna is matched to their respective feeding circuit, the equation can be written as:

$$|S21|^2 \sim \frac{P_r}{P_t} = G_t G_r \left(\frac{\lambda}{4\pi R}\right)^2 \left|\hat{\boldsymbol{\rho}}_{\mathbf{t}} \cdot \hat{\boldsymbol{\rho}}_{\mathbf{r}}\right|^2, \tag{1}$$

where G_t and G_r are the gains of the antennas, $\hat{\boldsymbol{\rho}}_{\mathbf{t}}$ and $\hat{\boldsymbol{\rho}}_{\mathbf{r}}$ are polarization unit vectors of the transmitting and receiving antennas, respectively, λ is the wavelength, and R is the distance between the two antennas. If we use a two-port measurement system, such as a network analyzer, $|S21|^2$ may be proportional to the power ratio. If the characteristics of the transmitting antenna and the distance R are known, the radiation pattern of the receiving antenna $\mathbf{E}_r$ can be obtained by the following relationship:

$$S21 \sim \mathbf{E}_r \cdot \hat{\boldsymbol{\rho}}_{\mathbf{t}}, \tag{2}$$

where $S21$ is what we measured using the two-port system. If the probe antenna and the AUT are connected to ports 1 and 2, respectively, $S21$ can be related to the radiation pattern of the AUT if a proper compensation method is used.

Similarly, when a scatterer is present in the far zone of an antenna, the backscattered field can be represented using the radar range equation [1]. For a monostatic antenna with no reflection loss, the equation can be written as:

$$|S11|^2 \sim \frac{P_r}{P_t} = G_a^2 \frac{\sigma}{4\pi}\left(\frac{\lambda}{4\pi R^2}\right)^2 \left|\hat{\boldsymbol{\rho}}_{\mathbf{a}} \cdot \hat{\boldsymbol{\rho}}_{\mathbf{s}}\right|^2, \tag{3}$$

where G_a is the gain of the antenna, σ is the radar cross section of the scatterer, and $\hat{\boldsymbol{\rho}}_{\mathbf{a}}$ and $\hat{\boldsymbol{\rho}}_{\mathbf{s}}$ are the polarization unit vectors of the antenna and the scattered field, respectively. The measured quantity $S11$ is related to the radiation pattern of the antenna, as follows:

$$S11 \sim \left(\mathbf{E}_a \cdot \hat{\boldsymbol{\rho}}_{\mathbf{s}}\right)^2. \tag{4}$$

If the scatter is responsive to a single polarization and its radar cross section is known, the one-way radiation pattern of the antenna can be obtained as follows:

$$\sqrt{S11} \sim \mathbf{E}_a \cdot \hat{\boldsymbol{\rho}}_{\mathbf{s}}. \tag{5}$$

If the antenna is connected to port 1, both transmitting and receiving, $\sqrt{S11}$ can be related to the radiation pattern of the AUT if a proper compensation method is used.

In the above descriptions, far-field conditions are assumed. However, Eqs. (2) and (5) can be applied to the measurement of the near-field of the AUT. The measured near-field data can be transformed into a far-field radiation pattern using an NTFT technique. In a two-port system, the field should be sampled with a half wavelength spacing or less, for a planar near-field scanning surface [7]. The NTFT requires two components that are orthogonal to each other on the scanning surface. Therefore, a far-field pattern can be obtained by using two different probe antennas, or by adjusting the orientation of one probe antenna.

Likewise, in the proposed one-port system, the field should be sampled with proper spacing. According to the Nyquist sampling theorem, sampled signals with less than a half wavelength can be properly reconstructed. In the case of a squared function, the phase velocity will be twice as fast as the original function. Therefore, a one-port measurement system using an NTFT technique requires space sampling with at least a quarter wavelength or less. Because the quantity of interest is the square root of what we measure, its phase could be considered as having 180° of uncertainty [8]. The phase can be restored using a two-dimensional phase unwrapping method [9]. For example, for $S11 = a\exp(j\psi)$, the phase is first unwrapped to $\varphi = \text{unwrap}_{2\text{-D}}$

($S11$) using both the amplitude and phase of what we measure, then, the NTFT input can be:

$$\mathbf{E}_a \cdot \hat{\boldsymbol{\rho}}_{\mathbf{s}} = \sqrt{a}\exp(j\varphi/2). \tag{6}$$

Similar to the two-port system, the NTFT technique requires two components that are orthogonal to each other on the scanning surface. Therefore, the far-field pattern can be obtained by using two different scatterers or adjusting the orientation of one scatterer and properly applying the compensation method to near-field data.

III. Scatterer Geometry and Compensation Method

In a two-port antenna measurement system, the measured near-field data contains probe-dependent characteristics. Thus, the far-field radiation pattern is improved by compensating for the probe-dependent characteristics [7]. Similarly, in the proposed one-port antenna measurement system, the far-field radiation pattern can be improved by compensating for the scatterer-dependent characteristics.

In this work, a linear wire scatterer was chosen because of its simple current distribution and linear polarization. Let us suppose that a wire scatterer is aligned along the z-axis, as shown in Fig. 2, and a plane wave of unit amplitude with an arbitrary direction of propagation $\hat{\mathbf{k}}^i$ is incident on the scatterer. Then, the current induced on the scatterer is dependent on only the θ component of the incident wave, and the shape of the current distribution should be essentially the same for a small scatterer. For a specific reference, current distribution, $\mathbf{J}_n$, a plane wave incident in a direction $\hat{\mathbf{k}}^i$ can be considered to induce the following current distribution:

$$\mathbf{J}_s\left(z,\hat{\mathbf{k}}^i\right) = c\left(\hat{\mathbf{k}}^i\right)\mathbf{J}_n(z), \tag{7}$$

where $c\left(\hat{\mathbf{k}}^i\right)$ is a function of the incident direction. If we can write the radiated field from the current distribution $\mathbf{J}_n$ as:

$$\mathbf{E}_n(\mathbf{r}) = -j\omega\int \mathbf{J}_n G(\mathbf{r})\,dv', \tag{8}$$

the scattered field due to wave incident in the $\hat{\mathbf{k}}^i$ direction can be written as:

$$\mathbf{E}_s\left(\mathbf{r},\hat{\mathbf{k}}^i\right) = c\left(\hat{\mathbf{k}}^i\right)\mathbf{E}_n(\mathbf{r}), \tag{9}$$

where $G(\mathbf{r})$ is the free-space Green's function.

The equation indicates that the scattered field has the same pattern, except for the amplitude, regardless of the direction of the incident wave. Since the compensation method is derived from these characteristics, the wire scatterer needs to be electrically small. If the other scatterer geometries are considered, they must meet the conditions above.

The scattering (re-radiation) pattern of the wire scatterer, having a wide beamwidth, linear polarization, and smooth shape without a side lobe, could be advantageous for scatterer compensation and phase restoration.

1. Scatterer Compensation

Fig. 3 shows the geometry of an AUT and a scatterer in isotropic and lossless media. The AUT at the coordinate origin is connected to a port, which is both transmitting and receiving, and the scatterer is in the plane $x = x_0$. Suppose that the current on the AUT is $\mathbf{J}_a$, which is produced by the source generator. When there is no scatterer, $\mathbf{J}_a$ produces the fields $\mathbf{E}_a$ and $\mathbf{H}_a$. When the scatterer is present, $\mathbf{J}_s$ is induced on the scatterer due to $\mathbf{E}_a$ and $\mathbf{H}_a$. Then $\mathbf{J}_s$ is reradiated to produce $\mathbf{E}_s$ and $\mathbf{H}_s$, and subsequently $\mathbf{J}_{as}$ is induced on the AUT due to $\mathbf{E}_s$ and $\mathbf{H}_s$. These are shown in Fig. 4(a). Higher-order interactions are ignored for simplicity of explanation.

In the simplified geometry described above, there are two states. $\mathbf{J}_a$, $\mathbf{E}_a$, and $\mathbf{H}_a$ are present for a state when there is no scatterer, and $\mathbf{J}_a + \mathbf{J}_s + \mathbf{J}_{as}$, $\mathbf{E}_a + \mathbf{E}_s + \mathbf{E}_{as}$, and $\mathbf{H}_a + \mathbf{H}_s + \mathbf{H}_{as}$ are present for the other state when there is a scatterer.

First, we show that what we measure on the scanning surface S_1 is electromagnetic power coupled between the AUT and the scatterer by applying the reciprocity theorem between the two states in the two regions. For the AUT volume V_a, which is enclosed by the closed surface S_a, the reciprocity applied for the two states can be described as [1, 10]:

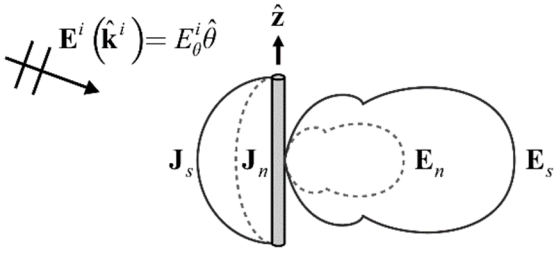

Fig. 2. Induced current distribution on a small wire scatterer corresponding to plane wave incidence.

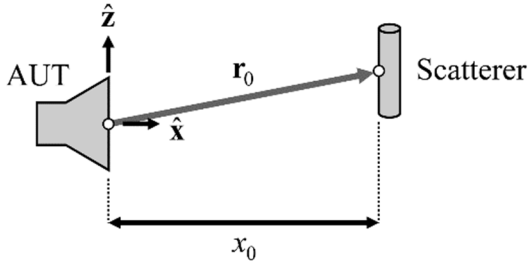

Fig. 3. Geometry and coordinate system for one-port antenna measurement.

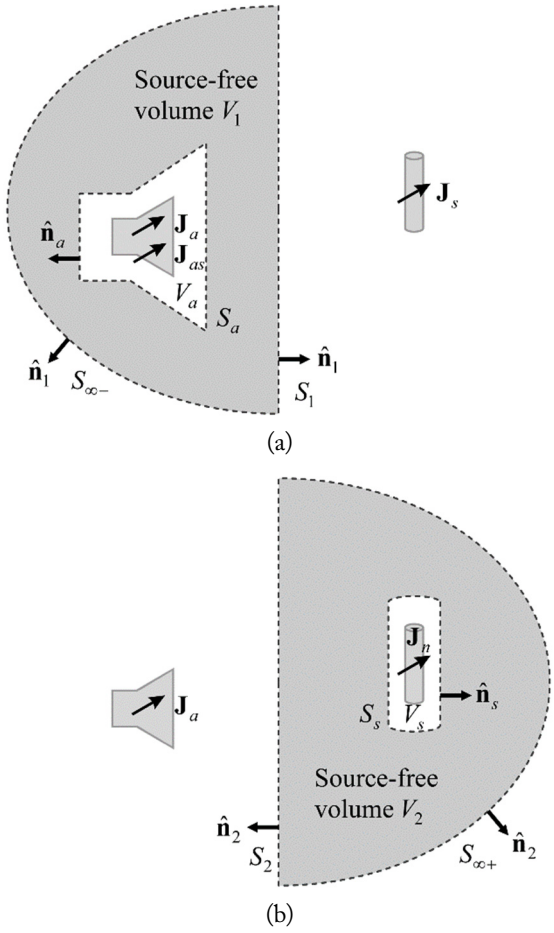

Fig. 4. Geometry definition for reciprocity: (a) volumes around the AUT and (b) volumes around the scatterer.

$$\oint_{S_a}\left\{\mathbf{E}_a\times\left(\mathbf{H}_a+\mathbf{H}_s+\mathbf{H}_{as}\right)-\left(\mathbf{E}_a+\mathbf{E}_s+\mathbf{E}_{as}\right)\times\mathbf{H}_a\right\}\cdot\hat{\mathbf{n}}_a\,da$$
$$=\int_{V_a}\mathbf{E}_a\cdot\left(\mathbf{J}_a+\mathbf{J}_s+\mathbf{J}_{as}\right)-\left(\mathbf{E}_a+\mathbf{E}_s+\mathbf{E}_{as}\right)\cdot\mathbf{J}_a\,dv. \quad (10)$$

The products $\mathbf{E}_a\cdot\mathbf{J}_{as}$, $\mathbf{E}_{as}\cdot\mathbf{J}_a$, $\mathbf{E}_a\times\mathbf{H}_{as}$, and $\mathbf{E}_{as}\times\mathbf{H}_a$ vanish due to the symmetry, and the induced current on the scatterer $\mathbf{J}_s$ does not exist in V_a [11]. Therefore, (10) can be simplified as:

$$\oint_{S_a}\left(\mathbf{E}_a\times\mathbf{H}_s-\mathbf{E}_s\times\mathbf{H}_a\right)\cdot\hat{\mathbf{n}}_a\,da$$
$$=-\int_{V_a}\mathbf{E}_s\cdot\mathbf{J}_a\,dv\triangleq P_a\left(\mathbf{r}_0\right), \quad (11)$$

where $\mathbf{r}_0$ is the position vector between the AUT and the scatterer. It can be thought that $P_a(\mathbf{r}_0)$ is proportional to the open-circuit voltage produced by the scattered field of the scatterer and could also be related to the S-parameter as follows:

$$P_a\left(\mathbf{r}_0\right)\sim S11\left(\mathbf{r}_0\right). \quad (12)$$

Next, we consider the reciprocity theorem between the two states for the source-free volume V_1, which is enclosed by S_1, $S_{\infty-}$, and S_a. In this source-free region, the reciprocity for V_1 can be written as:

$$\oint_{S_1+S_{\infty-}+S_a}\left\{\mathbf{E}_a\times\left(\mathbf{H}_a+\mathbf{H}_s+\mathbf{H}_{as}\right)\right.$$
$$\left.-\left(\mathbf{E}_a+\mathbf{E}_s+\mathbf{E}_{as}\right)\times\mathbf{H}_a\right\}\cdot\hat{\mathbf{n}}_1\,da=0. \quad (13)$$

Because all fields should be plane waves at $S_{\infty-}$, the integral $\int_{S_{\infty-}}\{\ \}\cdot\hat{\mathbf{n}}_1\,da=0$. We then obtain the following:

$$\int_{S_1}\left(\mathbf{E}_a\times\mathbf{H}_s-\mathbf{E}_s\times\mathbf{H}_a\right)\cdot\hat{\mathbf{n}}_1\,da$$
$$=\oint_{S_a}\left(\mathbf{E}_a\times\mathbf{H}_s-\mathbf{E}_s\times\mathbf{H}_a\right)\cdot\hat{\mathbf{n}}_a\,da=P_a\left(\mathbf{r}_0\right), \quad (14)$$

where $\hat{\mathbf{n}}_1=-\hat{\mathbf{n}}_a$. By applying the reciprocity theorem in the two regions, we obtained the same quantity $P_a(\mathbf{r}_0)$. Thus, the electromagnetic power coupled between the AUT and the scatterer passing through S_1 can be measured using $P_a(\mathbf{r}_0)$ at AUT.

Now, consider the geometry in Fig. 4(b), which shows the volume containing the scatterer. Suppose that we can model the scatterer as a wire antenna with a pair of imaginary terminals. An independent current source with I_n is placed across the terminals, producing the current $\mathbf{J}_n$ on the scatterer, which then produces $\mathbf{E}_n$ and $\mathbf{H}_n$. Applying the reciprocity theorem in volume V_s and in the source-free volume V_2, we can obtain the following two equations for the two volumes:

$$\oint_{S_s}\left(\mathbf{E}_a\times\mathbf{H}_n-\mathbf{E}_n\times\mathbf{H}_a\right)\cdot\hat{\mathbf{n}}_s\,da=\int_{V_s}\mathbf{E}_a\cdot\mathbf{J}_n\,dv, \quad (15)$$

and

$$\oint_{S_2+S_{\infty+}+S_s}\left(\mathbf{E}_a\times\mathbf{H}_n-\mathbf{E}_n\times\mathbf{H}_a\right)\cdot\hat{\mathbf{n}}_2\,da=0, \quad (16)$$

where the higher-order interactions are ignored. If the scatterer is electrically small, we can define I_n such that

$$\int_{V_s}\mathbf{E}_a\cdot\mathbf{J}_n\,dv=V_{oc}, \quad (17)$$

where V_{oc} is the open-circuit voltage across the terminals of the scatter due to fields $\mathbf{E}_a$ and $\mathbf{H}_a$. From (15), (16), and (17), we can obtain the following:

$$\int_{S_2}\left(\mathbf{E}_a\times\mathbf{H}_n-\mathbf{E}_n\times\mathbf{H}_a\right)\cdot\hat{\mathbf{n}}_2\,da=V_{oc}. \quad (18)$$

Note that the current induced on the scatter due to the fields $\mathbf{E}_a$ and $\mathbf{H}_a$ is a scaled version of $\mathbf{J}_n$, as shown in (7). In elaborating (17), $\mathbf{E}_a$ and $\mathbf{H}_a$ can be thought to induce an open-circuit voltage V_{oc} across the scatterer terminals. The current across the terminals of the scatterer could be V_{oc}/Z_s, where Z_s is the input impedance of the scatterer. Thus, (7) can be rewritten as:

$$\mathbf{J}_s=\alpha\frac{V_{oc}}{Z_s}\mathbf{J}_n, \quad (19)$$

where α is a proportionality constant. Accordingly, (9) and (14) can be rewritten as:

$$\alpha \frac{V_{oc}}{Z_s} \int_{S_1} \left(\mathbf{E}_a \times \mathbf{H}_n - \mathbf{E}_n \times \mathbf{H}_a \right) \cdot \hat{\mathbf{n}}_1 \, da = P_a(\mathbf{r}_0) . \tag{20}$$

Combining (18) and (20) gives:

$$\frac{\alpha}{Z_s} \left\{ \int_{S_1} \left(\mathbf{E}_a \times \mathbf{H}_n - \mathbf{E}_n \times \mathbf{H}_a \right) \cdot \hat{\mathbf{n}}_1 \, da \right\} \cdot \left\{ \int_{S_2} \left(\mathbf{E}_a \times \mathbf{H}_n - \mathbf{E}_n \times \mathbf{H}_a \right) \cdot \hat{\mathbf{n}}_2 \, da \right\} = P_a(\mathbf{r}_0) . \tag{21}$$

If we take that the surfaces S_1 and S_2 are identical, and $\hat{\mathbf{n}}_1 = -\hat{\mathbf{n}}_2$ in (21), using (12) we can obtain the following:

$$\int_{S_1} \left(\mathbf{E}_a \times \mathbf{H}_n - \mathbf{E}_n \times \mathbf{H}_a \right) \cdot \hat{\mathbf{n}}_1 \, da = \beta \sqrt{S11(\mathbf{r}_0)} \triangleq p_a(\mathbf{r}_0) , \tag{22}$$

where β is a proportionality constant.

Eq. (22) represents the relationship between the fields produced by $\mathbf{J}_a$ and $\mathbf{J}_n$ in the near zone. The above relationship can be transformed into a new relationship in the far field by using the plane wave spectrum and Fourier transform [11]. Here, we adopted the process described in [11] and [12]. Fields in the far zone can be represented using a spherical coordinate system (r, θ, ϕ), and the related wavenumber can be expressed as $\mathbf{k} = k \sin\theta \cos\phi \, \hat{\mathbf{x}} + k \sin\theta \sin\phi \, \hat{\mathbf{y}} + k \cos\theta \, \hat{\mathbf{z}}$. When the near-field plane S_1 is the yz-plane located at $x = x_0$, (22) can be written as:

$$E_\theta^a(\theta, \phi) E_\theta^n(\pi - \theta, \phi) - E_\phi^a(\theta, \phi) E_\phi^n(\pi - \theta, \phi) = C \sin\theta \cos\phi \exp(jk_x x_0) \cdot \int_{-\infty}^{\infty} \int_{-\infty}^{\infty} p_a(x_0, y, z) \exp\left(jk_y y + jk_z z \right) dy \, dz , \tag{23}$$

where $\mathbf{E}_a(\theta, \phi) = E_\theta^a \hat{\theta} + E_\phi^a \hat{\phi}$ is the radiation pattern of the AUT, $\mathbf{E}_n(\theta, \phi) = E_\theta^n \hat{\theta} + E_\phi^n \hat{\phi}$ is the scattering pattern of the small wire scatterer, which is assumed to be known, and C is a constant generated during the conversion process. Using two different scatterers, or adjusting the orientation of a single scatterer, the radiation pattern of the AUT can be calculated using a known pair of scattering patterns. The measured data according to the orientation of the scatterer are expressed as $p_{v,h}$, where the subscripts v and h imply that the scatterer is either aligned vertically or horizontally, respectively. Then, the radiation pattern of the AUT, ignoring the constant C, can be written as follows:

$$E_\theta^a(\theta, \phi) = \frac{\sin\theta \cos\phi}{\Delta(\theta, \phi)} \left\{ I_h(\theta, \phi) E_\phi^v(\pi - \theta, \phi) - I_v(\theta, \phi) E_\phi^h(\pi - \theta, \phi) \right\} , \tag{24}$$

and

$$E_\phi^a(\theta, \phi) = \frac{\sin\theta \cos\phi}{\Delta(\theta, \phi)} \left\{ I_h(\theta, \phi) E_\theta^v(\pi - \theta, \phi) - I_v(\theta, \phi) E_\theta^h(\pi - \theta, \phi) \right\} , \tag{25}$$

where

$$I_{v,h}(\theta, \phi) = \exp\left(jk_x x_0 \right) \cdot \int_{-\infty}^{\infty} \int_{-\infty}^{\infty} p_{v,h}(x_0, y, z) \exp(jk_y y + jk_z z) \, dy \, dz \tag{26}$$

and

$$\Delta(\theta, \phi) = E_\theta^h(\pi - \theta, \phi) E_\phi^v(\pi - \theta, \phi) - E_\theta^v(\pi - \theta, \phi) E_\phi^h(\pi - \theta, \phi) . \tag{27}$$

Here, $\mathbf{E}_v(\theta, \phi) = E_\theta^v \hat{\theta} + E_\phi^v \hat{\phi}$ and $\mathbf{E}_h(\theta, \phi) = E_\theta^h \hat{\theta} + E_\phi^h \hat{\phi}$ are the scattering patterns for vertically and horizontally aligned scatterers, respectively. The processes represented in (23) through (27) are different from those in [11] and [12] as follows:

(i) unwrapped square root of $S11$ is used instead of $S21$,
(ii) the quantity $S11$ is obtained from the AUT, and
(iii) the scattering pattern of the scatterer is used instead of the radiation pattern of the probe antenna.

IV. EXPERIMENT AND VALIDATION

To verify the performance of the one-port near-field antenna measurement technique with a small wire scatterer, we performed a radiation pattern measurement. Fig. 5 shows the measurement setup. A 2 × 1 horn antenna was used as an AUT because it has significantly different near- and far-field patterns. A 0.68 cm long wire with a diameter of 0.5 mm was used as a scatterer. The length of the wire was chosen to be a half wavelength at the highest frequency of interest. A robot arm scans the scatterer over the near-field scanning surface, whereas a network analyzer measures the $S11$ at frequencies from 15 to 22 GHz at each grid point. The scanning surface was 5 cm from the AUT and 20 cm × 20 cm in area with a 0.2 cm grid spacing. The measurement area was empirically chosen such that the variation over the main lobe is relatively small. The spacing needs to be less than a quarter wavelength according to the Nyquist theorem, which is 0.34 cm. In practice, slightly less spacing interval is desired, and we chose 0.2 cm for simplicity. To reduce the reflections from the robot arm, the scatterer is located at the top of a 50 cm high truncated expanded polystyrene (EPS) cone, whose bottom is attached to the robot arm.

In many cases, the AUT may not be matched to the driving circuit. Therefore, the reflections from the input port could be significant. The AUT consists of two horn antennas, cables, and a power divider. The time-domain waveform shows the internal reflections from these components, as shown in Fig. 6(a). To

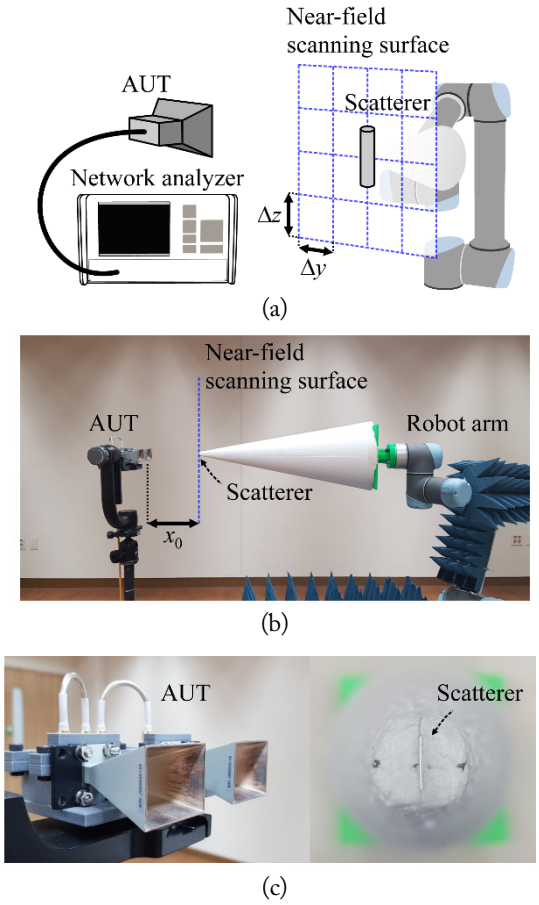

Fig. 5. One-port near-field antenna measurement technique validation: (a) concept of measurement setup, (b) photograph of the AUT and scatterer arrangement, and (c) photographs of the AUT and scatterer.

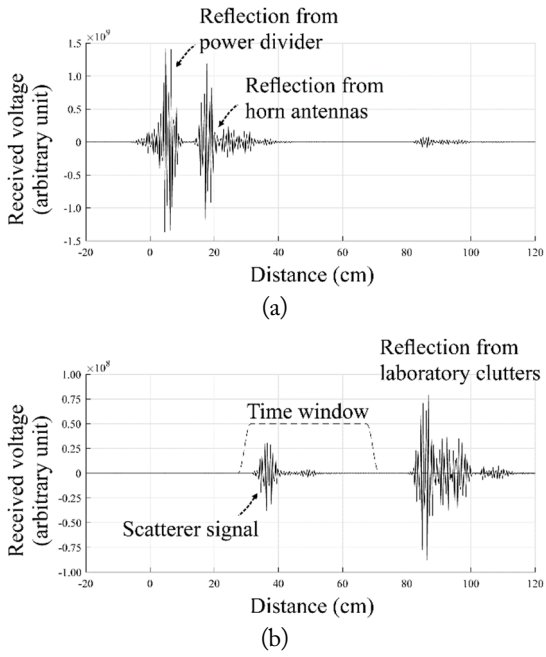

Fig. 6. Time domain waveform of measured $S11$ (a) including the internal reflections of the AUT and (b) without the internal reflections.

remove these internal reflections, we measure the differences between the signal with the scatterer, $S11$, and the signal without the scatterer, $S11'$. Because both $S11$ and $S11'$ contain the same internal reflections, we can obtain the signal without the internal reflections from $\Delta S11 = S11 - S11'$. The time-domain waveform of $\Delta S11_v$ for $\mathbf{r}_0 = (x_0, 0, 0)$ is shown in Fig. 6(b). To further reduce the signals from laboratory clutter, such as the robot arm, walls, and floors, time gating was applied.

Fig. 7 shows the measured amplitudes and phases of the near-field data from the vertically aligned scatterer at 18 GHz. Fig. 8 shows the far-field radiation patterns obtained from the proposed compensation method at 18 GHz. The phases were restored using the weighted least-squares 2D phase unwrapping method [9]. Figs. 7(a), 7(b), and 8(a) were obtained by having the main beam of the AUT aligned to the x-axis, and Figs. 7(c), 7(d), and 8(b) were obtained by tilting the main beam by 20° in

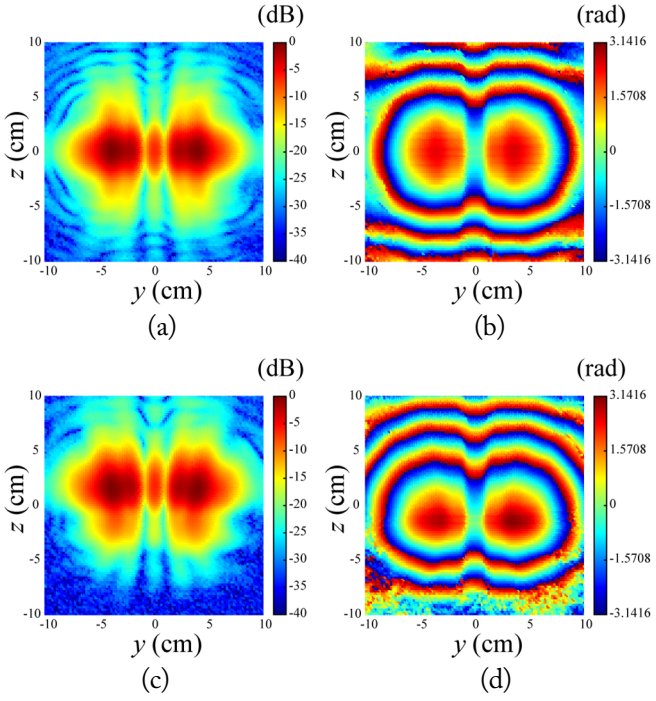

Fig. 7. Amplitude (a, c) and phase (b, d) of near-field data p_v: (a) and (b) are for 0° tilted AUT, and (c) and (d) are for 20° tilted AUT.

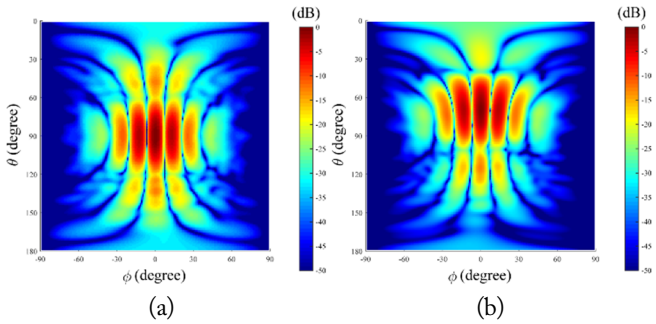

Fig. 8. Radiation patterns of 2 × 1 horn antenna in the θ–ϕ domain: (a) 0° tilted case and (b) 20° tilted case.

the E-plane. The figures show the near- and far-field pattern differences and the well-transformed radiation patterns with the main beam in the corresponding tilt angles.

In order to show the accuracy of the proposed method, the radiation patterns obtained from the proposed method are compared with those measured in a conventional direct measurement facility, which is a 16 m × 11 m × 9.5 m commercial anechoic chamber. Fig. 9 shows the radiation patterns of the AUT in both the E- and H-planes at 18 GHz. The red solid lines show the conventional measurement, and the blue dashed lines and black dotted lines show the proposed measurement with and without the proposed compensation, respectively. As shown in the figures, the proposed measurements, both with and without the proposed compensation, agree well with the conventional measurement within the range of ±30° from the center. Because the planar scanning surface is suitable for the directive antennas, only the patterns near the center are considered accurate. Nevertheless, the compensation method still shows the improvement in the off-center region, so the agreement is closer to the proposed compensation.

Thus, the proposed one-port near-field antenna measurement technique was validated for a planar scanning surface.

V. Conclusion

In this work, a one-port near-field antenna measurement technique with a small wire scatterer was proposed. In the conventional near-field measurement technique, a probe antenna is scanned in the near-field scanning surface with a sampling interval of less than a half wavelength. The *S*21 parameter was measured between the probe and AUT. The data obtained in the near-field were transformed to the far-field pattern. The probe radiation pattern was compensated for better measurements. However, in the proposed technique, a wire scatterer is scanned with an interval of less than a quarter wavelength, and the measurement is made only at the port of the AUT. The 180° phase uncertainty was removed by applying a 2D phase unwrapping method. The data obtained in the near-field were transformed to a far-field pattern. The scatterer scattering pattern was compensated for better measurements.

The proposed measurement technique was validated by measuring the radiation pattern of an AUT, which is a 2 × 1 horn antenna. The far-field radiation pattern obtained using the proposed technique was compared with that obtained from a conventional commercial anechoic chamber. It was shown that they agree well, especially in the region near the center, which is expected because of the nature of the rectangular near-field scanning surface. In future studies, the precision of the proposed technique will be further improved by enhancing the scattered signal using other types of scatterers.

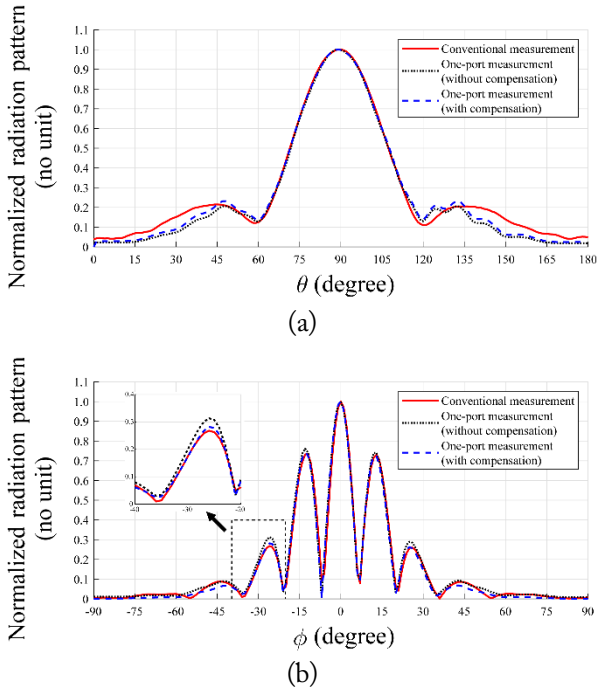

Fig. 9. Radiation pattern cuts in the principal (a) E-plane and (b) H-plane.

This work was supported in part by the National Radio Research Agency of Korea, under the project entitled "Development of rapid antenna measurement technique for antennas with new radio technology."

References

[1] C. A. Balanis, *Antenna Theory: Analysis and Design*, 3rd ed. Hoboken, NJ: John Wiley & Sons, 2005.

[2] R. J. Marhefka and W. D. Burnside, "Antennas on complex platforms," *Proceedings of the IEEE*, vol. 80, no. 1, pp. 204-208, 1992.

[3] J. Hasch, E. Topak, R. Schnabel, T. Zwick, R. Weigel, and C. Waldschmidt, "Millimeter-wave technology for automotive radar sensors in the 77 GHz frequency band," *IEEE Transactions on Microwave Theory and Techniques*, vol. 60, no. 3, pp. 845-860, 2012.

[4] R. Justice and V. Rumsey, "Measurement of electric field distributions," *IRE Transactions on Antennas and Propagation*, vol. 3, no. 4, pp. 177-180, 1955.

[5] T. Calazans, H. D. Griffiths, A. L. Cullen, D. E. N. Davies, and R. Benjamin, "Antenna radiation pattern measurement using a near-field wire scattering technique," *IEE Proceedings-Microwaves, Antennas and Propagation*, vol. 145, no. 3, pp. 263-267, 1998.

[6] J. C. Bolomey, B. J. Cown, G. Fine, L. Jofre, M. Mostafavi,

D. Picard, J. P. Estrada, P. G. Friederich, and F. L. Cain, "Rapid near-field antenna testing via arrays of modulated scattering probes," *IEEE Transactions on Antennas and Propagation*, vol. 36, no. 6, pp. 804-814, 1988.

[7] *IEEE Recommended Practice for Near-Field Antenna Measurements*, IEEE Standard 1720-2012, 2012.

[8] J. C. Bolomey and F. E. Gardiol, *Engineering Applications of the Modulated Scatterer Technique*. Boston, MA: Artech House, 2001.

[9] D. C. Ghiglia and M. D. Pritt, *Two-Dimensional Phase Unwrapping: Theory, Algorithms, and Software*. New York, NY: Wiley, 1998.

[10] M. Stumpf, *Electromagnetic Reciprocity in Antenna Theory*. Hoboken, NJ: John Wiley & Sons, 2018.

[11] D. Paris, W. Leach, and E. Joy, "Basic theory of probe-compensated near-field measurements," *IEEE Transactions on Antennas and Propagation*, vol. 26, no. 3, pp. 373-379, 1978.

[12] E. Joy, W. Leach, and G. Rodrigue, "Applications of probe-compensated near-field measurements," *IEEE Transactions on Antennas and Propagation*, vol. 26, no. 3, pp. 379-389, 1978.

Seunggyu Yang

received the B.S. degree in radio-frequency engineering from Korea Maritime and Ocean University, Busan, South Korea, in 2013, and the M.S. degree in mechatronics engineering from the Gwangju Institute of Science and Technology, Gwangju, South Korea, in 2015, where he is currently pursuing the Ph.D. degree.

Kangwook Kim

received the B.S. degree in electrical engineering from Ajou University, Suwon, South Korea, in 1997, and the M.S. and Ph.D. degrees in electrical and computer engineering from the Georgia Institute of Technology (GA Tech), Atlanta, GA, USA, in 2001 and 2003, respectively, where he focused on the design, analysis, and measurement of pulse-radiating antennas. From 1999 to 2003, he was a Graduate Research Assistant with the School of Electrical and Computer Engineering, GA Tech, where he was involved in the research of ultrawideband and pulse-radiating antennas. From 2003 to 2005, he was a Post-Doctoral Fellow with GA Tech, where he was involved in multimodal landmine-detection system research. From 2005 to 2006, he was with the Samsung Advanced Institute of Technology, Suwon, South Korea. In 2006, he joined the Faculty of the Gwangju Institute of Science and Technology, Gwangju, South Korea, as an Assistant Professor. His current research interests include millimeter-wave antennas, remote sensing of concealed objects, and ultrawideband electromagnetics.